Oxidative chemical vapor deposition of polypyrrole onto carbon fabric for flexible supercapacitive electrode material

Dianatdar, Afshin; Mukherjee, Adrivit; Bose, Ranjita K.

Published in:
Synthetic Metals

DOI:
10.1016/j.synthmet.2023.117444

Publication date:
2023

Synthetic Metals 298 (2023) 117444

Contents lists available at ScienceDirect

Synthetic Metals

journal homepage: www.elsevier.com/locate/synmet

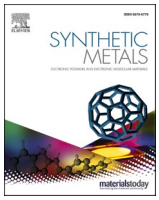

Oxidative chemical vapor deposition of polypyrrole onto carbon fabric for flexible supercapacitive electrode material

Afshin Dianatdar, Adrivit Mukherjee, Ranjita K. Bose *

Department of Chemical Engineering, Engineering and Technology Institute Groningen (ENTEG), University of Groningen, 9747AG Groningen, the Netherlands

ARTICLE INFO

Keywords:
Polypyrrole
Flexible supercapacitor
Oxidative chemical vapor deposition (CVD)

ABSTRACT

Polypyrrole has been a promising conjugated polymer for application in electrochemical energy storage devices. One primary feature is its pseudocapacitive behavior, which makes it suitable for hybridization with traditional carbon-based electrical double layer capacitive materials. The processing condition for such a hybridization is a critical aspect for the electrode performance in long term. Oxidative chemical vapor deposition was used to deposit polypyrrole onto 3D carbon fiber fabric. This allowed uniform and conformal deposition of polypyrrole on individual fibers as well as a control over its thickness depending on the reaction time. The obtained composite was characterized for electrochemical energy storage application using cyclic voltammetry and galvanostatic charge discharge measurements. Additionally, the stability of the polypyrrole-carbon fiber electrode was tested using microscopy and energy dispersive spectroscopy in order to obtain insights into physical and chemical degradation of polypyrrole during electrochemical aging. Results showed thickness-dependence of electrode stability, tuning of which in the correct voltage window is necessary for optimal long-term performance.

1. Introduction

The rapid growth of energy demand combined with ever-increasing environmental concerns in recent decades has prompted a great deal of research, improvement, and adaptations in electrical energy technologies. One of the most important aspects of these technologies relate to energy storage systems, which convert electricity into an alternative carrier of energy and re-convert it back to electricity on demand [1,2]. Among different systems serving this purpose, electrochemical energy storage devices play an important role [3]. These devices include fuel cells, batteries, and capacitors [4]. The first two provide high energy and low power while the latter provides a high power and a low energy. As a step towards filling the gap between these two categories, supercapacitors were developed with an intention of providing high power and energy at the same time [4,5]. Their structure resembles that of batteries with two electrodes sandwiching an electrolyte (liquid or solid) and separated by an insulating layer [6].

Supercapacitors are categorized into two groups: (i) electrical double-layer capacitors (EDLC) in which the charge formation is the result of physical interaction between the electrodes and electrolytes, and (ii) pseudocapacitors in which the mechanism of charge formation is dominated by repetitive redox reactions [7,8]. EDLCs have already established themselves as a mature field and found their way into commercial applications. High porosity carbon-based materials are often used for this purpose [9]. Pseudocapacitive electrodes on the other hand are still in research phase. They are mainly classified in two groups of metal oxides (e.g. MnO_2) and conjugated polymers such as polythiophene, polyaniline, polypyrrole (PPy) [10]. Metal oxides offer a higher capacitance and energy density compared to conjugated polymers. However, they suffer from low conductivity, agglomeration at high loading, poor cycling stability, and are vulnerable to mechanical degradation. Conjugated polymers on the other hand are comparably more flexible with a higher conductivity and could be readily synthesized from abundant sources. Both these types of electrodes are under research and development and not yet in commercial production [11].

Although polymers in general have been used in all three components of an electrochemical capacitor – namely electrode, electrolyte, and separator - conjugated polymers in particular are often used in only electrodes [12–14]. Immense research in recent decades have focused on their chemical modification or physical blending with other electrode materials (carbon-based and/or metal oxides) to improve their capacitance [15]. The most popular conjugated polymers are polyaniline,

* Corresponding author.
E-mail address: r.k.bose@rug.nl (R.K. Bose).

https://doi.org/10.1016/j.synthmet.2023.117444
Received 11 November 2022; Received in revised form 27 June 2023; Accepted 3 August 2023
Available online 7 August 2023

polythiophene, and polypyrrole, which have been used to modify electrode materials in these works [16–22]. A large amount of data now exists using different conjugated polymers, often combined with other electrode materials using different processing methods and tested with different electrolyte environments. However, a lack of standard test procedure, as for example in the case for EDLCs[23], makes it a challenge to evaluate their potential for real life application. Thus, it is only by comparing between different systems that one could evaluate performance of a developed electrode. This however is challenging as often one or more parameters are varied – e.g., type and concentration of electrolyte, electrode formulation, scale of study- between different research papers, making the evaluation process tedious and uncertain.

Despite these challenges, one particular aspect is generally agreed upon: conjugated polymers are not stable for a long-term use [24,25]. This necessitates more research about the degradation of conjugated polymers and possible ways to alleviate it. The main reason recognized for the deterioration of conjugated polymer electrodes is constant volumetric expansion and shrinkage as a result of repetitive ion insertion and de-insertion during oxidation and reduction. Such a volumetric change causes electrode cracking and mechanical failure and possibly blockage of charge transfer channels between the electrolyte and electrode. Other reasons impacting stability include voltage working range, current density, type of electrolyte, nature of the polymer (in this case PPy), morphology of the electrode, and usage temperature [25].

There have been different approaches to alleviate the above challenges. One successful strategy was to embed conjugated polymers within a flexible substrate enhancing the tolerance for volumetric change [26–28]. An alternative strategy has been the deposition of a thin protective layer on top of conjugated polymer and thereby placing a physical barrier between the electrode and electrolyte.[29,30] Also, controlling and fine-tuning the nanostructure of conjugated polymer-based electrodes have shown to be another strategy to improve stability via more favorable ionic diffusion paths within electrode-electrolyte sites [31]. Optimizing the voltage range and current density are then additional measures to make sure that the supercapacitive electrode is being used in its optimal operational condition [25].

Another critical aspect about the stability of conjugated polymer electrodes is their thickness. There are a few reports focusing on thickness-dependent electrochemical energy storage behavior of conjugated polymers. Patil et al. developed polyvinyl alcohol/polyaniline (PANI) electrode, varied the PANI thickness between 0.3 and 2.3 μm and obtained the optimal specific capacitance at thickness of 0.88 μm [32]. Moreover, the same electrode thickness showed the highest stability during 20,000 cycles of charge-discharge. Investigating their results, they concluded that as the PANI thickness was increased, the porosity at % of PANI increased, facilitating “ion diffusion resistance” as they put it. In another work on PANI with thickness range between 0.5 and 11 μm, it was observed that the highest gravimetric specific capacitance was associated with the thinnest PANI electrode, while the stability enhanced with electrode thickness of 4.5 μm and reduced afterwards [33]. This is in agreement with [32]. In general, the loss of capacitance in thicker coatings is due to an increased film resistance and slow ion diffusion into solid matter, which negatively impact charge transfer [34]. After all it is worth mentioning, the that the above numbers are relevant only while considering the length-scale of the structure the electrode material. In other words, in an electrode with nano-scale structural features, the micro-scale polymer coating would disrupt the network. This is the reason that in some other reports, thicknesses in order of 5–10 nm were suggested as the optimal coating thickness [35].

Nonetheless, for a composite of conjugated polymer with carbon-based materials, an intimate contact between the two is very important to ensure efficient charge transfer and avoid failure at their interface. A failure at the interface may delaminate polymer from its underlining substrate, which impedes the volumetric breathing during cycling [25,36,37]. Providing a conformal and intimate contact is particularly challenging for traditional solvent-based processing techniques such as chemical bath deposition, casting methods, and electrodeposition, due to surface dewetting and interfacial tension effects, particularly for porous carbon-based substrates [38–41]. The failure of the aforementioned coating techniques to provide conformal coating on top of individual carbon particles/fibers, further alters the nano/micro-morphology of these materials, which negatively impacts the electrode performance [42].

In this regard, oxidative chemical vapor deposition (oCVD) has been reported as a solvent-free method for deposition of conjugated polymers uniformly and conformally onto porous carbon-based substrates. The Gleason group first reported PEDOT-grown aligned carbon nanotube using oCVD, which resulted in significant life cycle stability compared with PEDOT-CNT processed with other methods [42–45]. Other researchers have used oCVD for integration of PANI and poly (3-mthyl thiophene) with carbon-based materials for application as supercapacitive electrodes [38,46,47].

In light of the above considerations, the present work aims to provide a preliminary investigation for oCVD-grown polypyrrole (PPy) into porous and flexible carbon fabric for the first time. PPy has been selected as it is a well-known and promising choice among conjugated polymers as a main category of pseudocapacitive materials [17]. We have chosen a commercially available carbon fiber fabric as a flexible substrate to enable the PPy-carbon electrode to mitigate the constant volumetric change effect. This is further reassured by well-controlled conformal and uniform PPy deposition on the surface of individual fibers within the fabric network, preserving the fabric initial micro-morphology of the PPy-coated carbon fabric composite. Deposition time was used to control the thickness and morphology of PPy layer. The PPy-carbon fabric was then degraded with an accelerated aging protocol to assess the effect of PPy thickness on its long-term stability. Following this, the optimal voltage range was then determined, and the resultant electrode was electrochemically characterized using cyclic voltammetry (CV), galvanostatic charge-discharge measurement (GCD), and thermal stability test. The results are critically discussed and compared with other reports.

2. Experimental

2.1. Materials

Pyrrole (> 99%) was purchased from TCI Europe. Antimony pentachloride ($SbCl_5$, > 98%), Lithium perchlorate (99.99%, battery grade), H_2SO_4 (1 mol L^{-1}), and propylene carbonate (PC) were purchased from Sigma Aldrich and used as received. Single-side polished silicon wafers with orientation of 100 (N/Ph), thickness of 180–220 μm was bought from Sil’Tronix (France); SIGRACELL battery fabric GFD 2.5 E.A, and Sigraflex L02510TH (0.25 mm thickness, 1 g cm^{-3} density, purity >=99.85%) were bought from SGL Carbon GmbH (Germany).

2.2. Electrode development

PPy electrodes were developed by oCVD of PPy on SGL GFD 2.5 E.A (hereafter called carbon fabric). The carbon fabric was placed on the bottom of the reactor. The bottom of the was heated to 40 °C and controlled by electrical elements from the outside. To avoid the condensation of the reactants, all feed through lines as well as the reactor body were heated up to 110 °C and 40 °C, respectively. The reactor pressure was monitored by pressure transducer (MKS, model 622C11TBE) and controlled by a throttle valve (MKS, model 653B-1–40–1).

For all reactions, the monomer and the oxidant were heated to 60 °C and controllably metered into the reactor via Swagelok valves from two different reactor walls perpendicular to each other. In all depositions, N_2 was used as the diluent gas as well as the carrier gas to improve the delivery of the oxidant into the reactor. For PPy deposition, pyrrole flow

Table 1
An overview of prepared electrodes.

Electrode	PPy deposition time (min)	Substrate treatment
C1-PPy30	30	-
C1-PPy90	90	-
C2-PPy30	30	Thermally activated
C2-PPy60	60	Thermally activated
C2-PPy90	90	Thermally activated

rate of 2.5 standard cubic centimeters per minute (sccm), $SbCl_5$ flow rate of 0.5 sccm, and N_2 flow rate of 2 sccm was used. Two sets of electrodes were prepared. The first set used the carbon fabric as received with PPy deposition time of 30 and 90 min. The electrodes are called C1-PPy30 and C1-PPy90, respectively. For the second set of electrodes, the carbon fabric was first thermally oxidized at 400 °C for 24 h and then coated with PPy for 30, 60, and 90 min. The developed electrodes are called C2-PPy30, C2-PPy60, and C2-PPy90, respectively. The composition and pre-treatment of the electrodes are shown in Table 1. All electrodes were rinsed with acetone to remove unreacted monomer and oxidant at the surface, dried at 100 °C and finally stored in argon environment before further characterizations.

2.3. Characterization

Fourier-transform infrared spectroscopy (FTIR) (Shimadzo IRTracer) in transmission mode was used to characterize the chemical structures of the deposited coatings. Spectra were averaged over 128 scans with a scan resolution of 4 cm^{-1}. Scanning electron microscopy (Nova Nano-SEM 650) was used for morphology study of the developed electrodes along with estimation of deposited PPy coatings in different experiments. The electrodes were coated with gold (10 nm); measurements were conducted with a working distance of 5 mm and an acceleration voltage of 10 kV. A three-electrode cell configuration was used for electrochemical characterization of single electrodes. For cyclic voltammetry (CV) and galvanostatic charge-discharge (GCD) measurements, a rectangular PPy-coated carbon fabric (10 mm × 10 mm) was used as the working electrode (WE), Ag/AgCl (Metrohm) as reference electrode (RE) and platinum sheet (surface = 1 cm^2, Metrohm) as counter electrode (CE) using an Autolab PGSTAT306N potentiostat.

Electrochemical experiments were conducted in an undivided cell in ambient environment using either of the three electrolyte systems, namely aqueous: H_2SO_4 (1 mol L^{-1}), organic: $LiClO_4$ in PC (0.25 mol L^{-1}); *I-V* curves were normalized by dividing the current per surface of exposed PPy-coated carbon fabric. Areal specific capacitance values were calculated from galvanostatic charge-discharge experiments as:

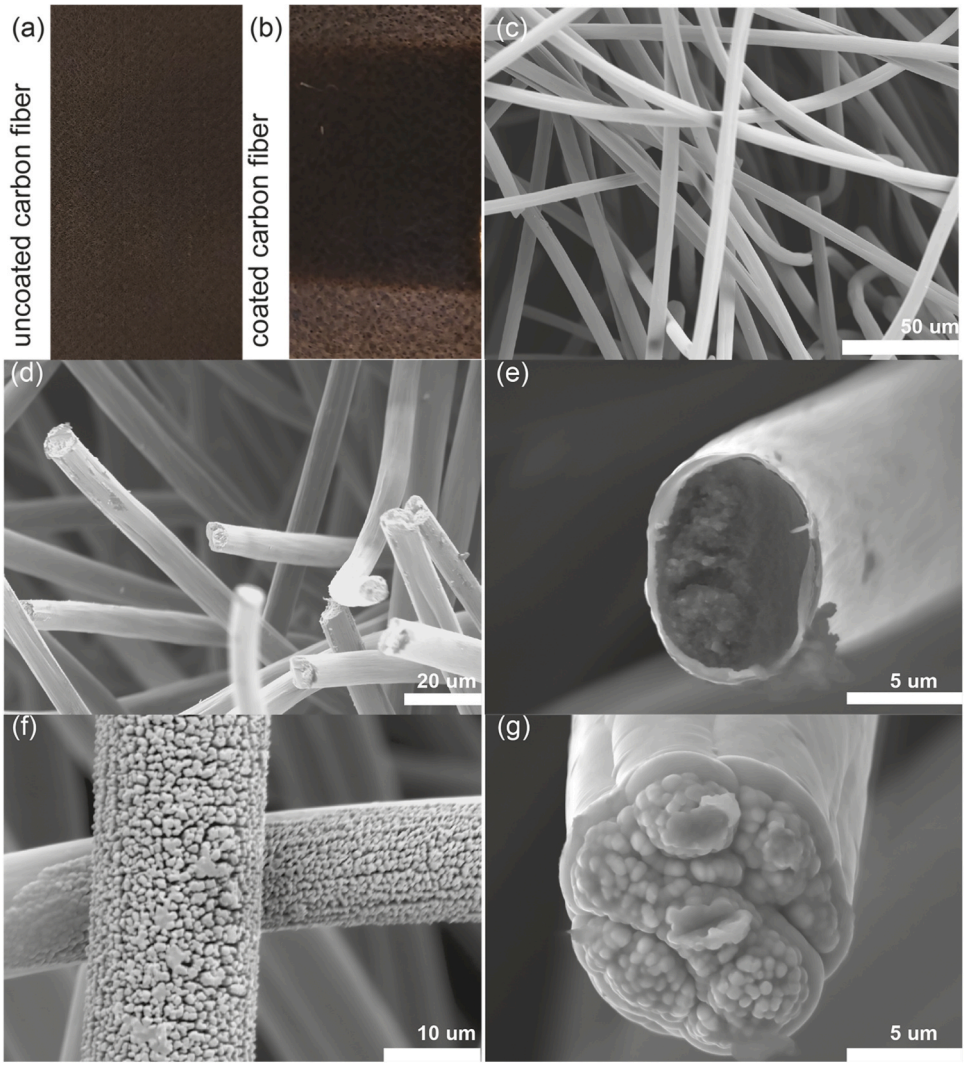

Fig. 1. Optical micrographs of carbon fabric (a) before coating; (b) after coating with PPy for 90 min; SEM images of (c) bare carbon fabric; (d, e) carbon fabric coated by PPy for 30 min: C1-PPy30; and (f, g) carbon fabric coated with PPy for 90 min: C1-PPy90.

Table 2
Experimental conditions of synthesis of PPy with high conductivity.

	Conductivity (S cm^{-1})	f_{SbCl5} (sccm)	$f_{pyrrole}$ (sccm)	f_{N2} (sccm)	Deposition Temperature (°C)	Vacuum pressure (mTorr)
Method 1	180	1.25	2.5	1.25	40	500
Method 2	155	0.5	2.5	2	40	300

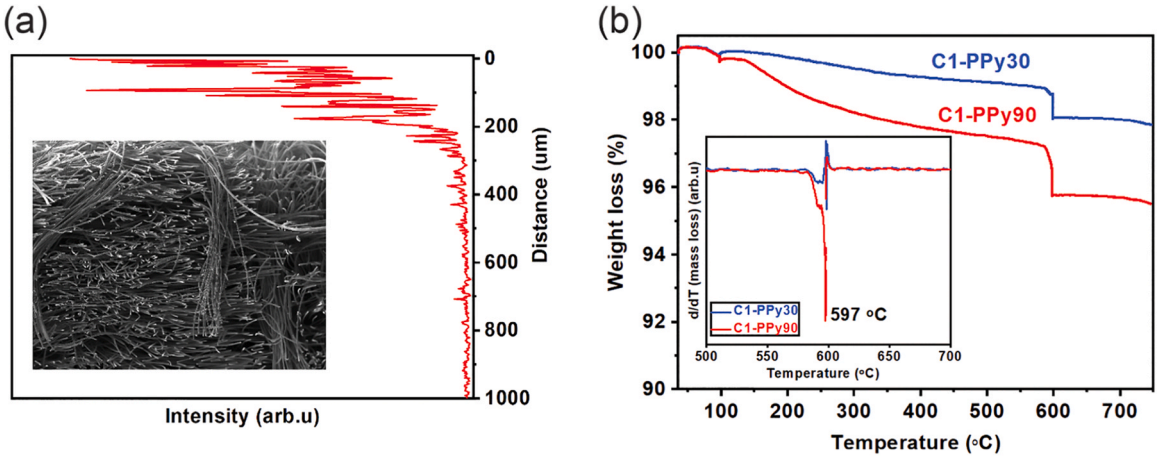

Fig. 2. (a) EDS of Cl(K) from cross section of C1-PPy90 starting from the outer surface exposed inside the reactor (top to bottom); (b)TGA of C1-PPy30 and C1-PPy90 between 35 and 750 °C.

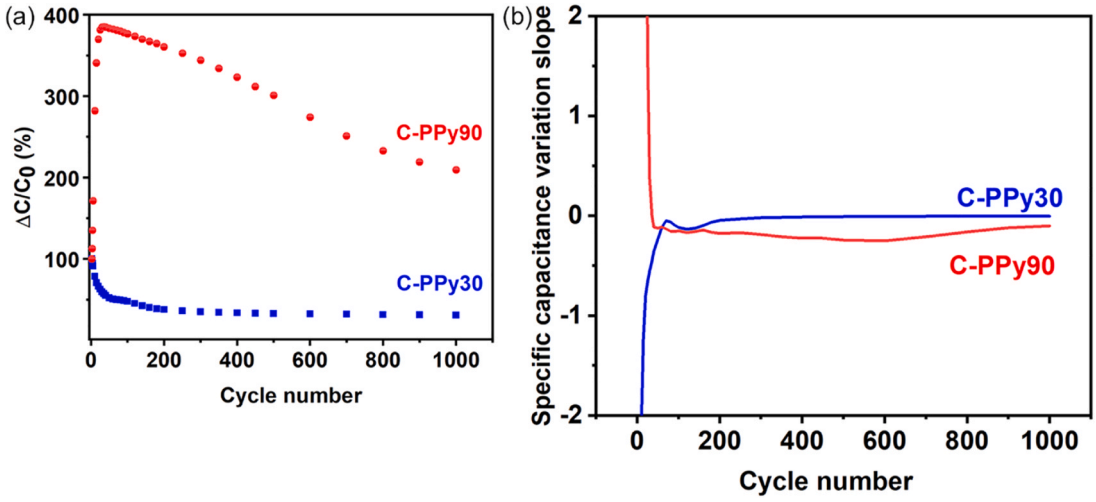

Fig. 3. (a) The change in areal specific capacitance of C1-PPy30 and C1-PPy90; (b) the slope of capacitance evolution during 1000 CV cycles. 1 cm^2 of either C1-PPy30 or C1-PPy90 were used as WE, the voltage was varied between − 1–1 V in PC/$LiClO_4$ (0.25 mol L^{-1}) as electrolyte.

Areal Specific Capacitance from GCD (mF cm^{-2}) $C = I\Delta t/S\Delta V$ (1)

Where I is the applied current, Δt is the discharge time, S is the exposed surface area of electrode. For certain experiments, the integration of I-V curve from CV measurements were used to monitor the evolution of areal specific capacitance, in accordance with Eq. (2):

$$\text{Areal Specific Capacitance from CV}(\text{mFcm}^{-2})\text{C} = \frac{\int I \quad dV}{2S \quad Vs\Delta V} \tag{2}$$

Where V_s is the scan rate.

3. Results and discussion

3.1. PPy-carbon fabric electrode development

The carbon fabric was coated by PPy using oCVD during 30 and 90 min and images before and after coating are provided in Fig. 1a/1b. It is important to prepare highly conductive PPy coating for better performance. According to previous work from our group[48], it was found that two particular deposition methods resulted in highest conductivities (Table 2). Although *Method 1* provides a bit higher conductivity, we continued with *Method 2* as the polymerization method on carbon fabric due to a lower ratio of oxidant to monomer flow rate (0.2 vs. 0.5) as well as lower pressure (300 mTorr vs. 500 mTorr), both resulting in a lower deposition rate and hence diffusion of the reactants into the porous network.

Fig. 1 shows the SEM graphs of the developed electrodes. As could be observed in Fig. 1b, c and d, the carbon fibers are uniformly and conformally coated with PPy of smooth surface morphology. When the coating was continued for longer time of 90 min, the grown PPy surface morphology, shown in Fig. 1f and g, becomes similar to that of known globular and cauliflower-like [49–51]. However, a difference is that there is clear space between every few globules.

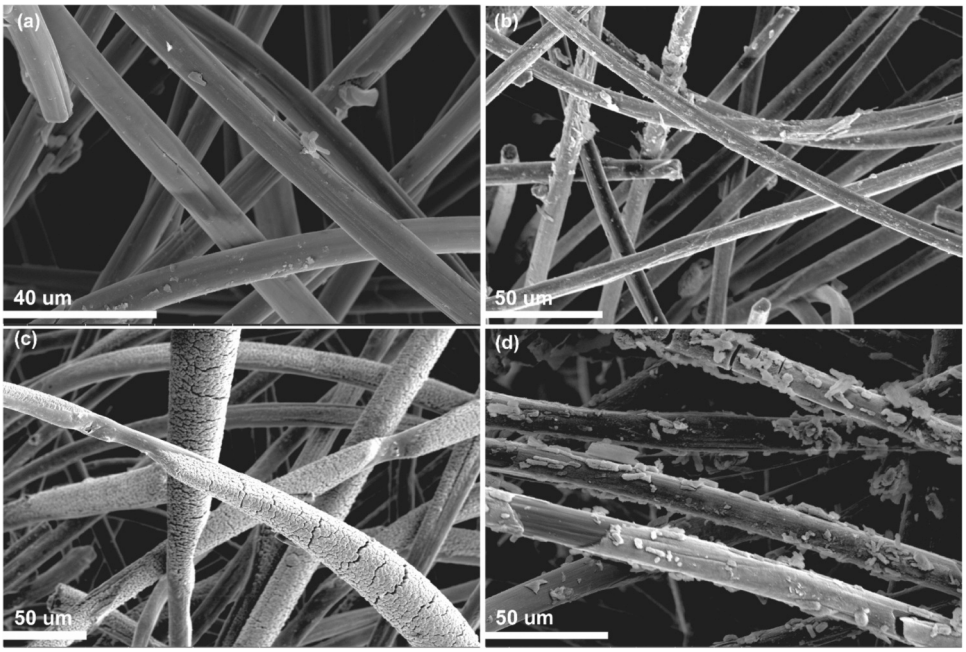

Fig. 4. SEM graphs for C1-PPy30 electrode cycled for (a)100 times (b) 1000 times, (b) C1-PPy30 CV1000; the SEM graphs for C1-PPy90 electrode cycled for (c) 100 times, and (d) 1000 times. A three-electrode cell was used for the experiment; $LiClO_4$/PC (0.25 mol L^{-1}) was used as the electrolyte and the cycling conducted between − 1–1 V.

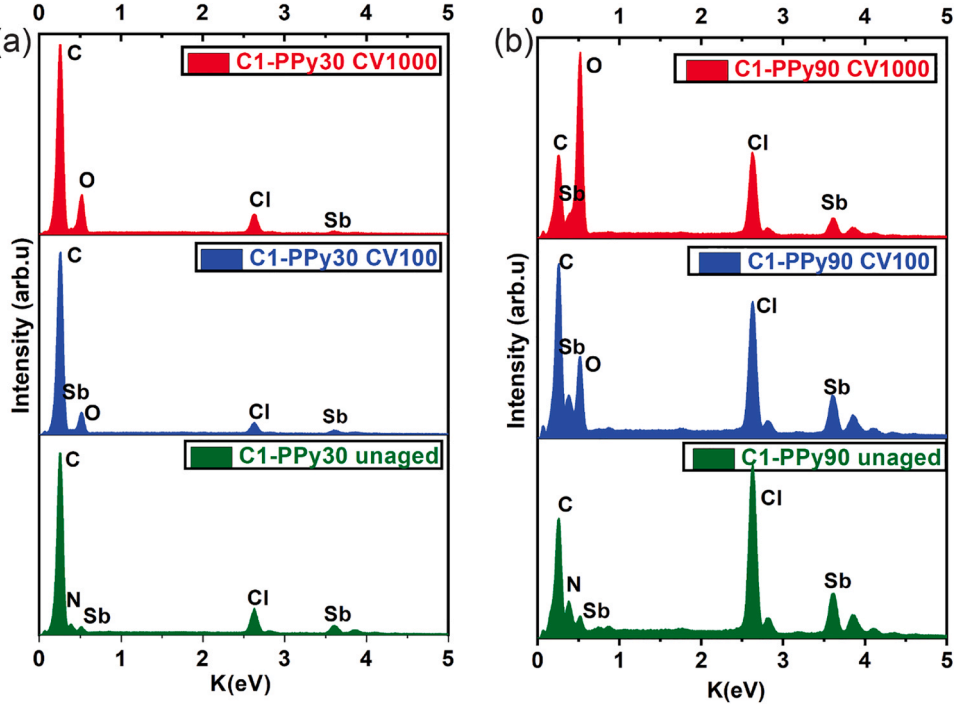

Fig. 5. EDS results showing evolution of carbon, nitrogen, antimony, and chlorine during 100 and 1000 cycles for (a) C1-PP30, and (b) C1-PPy90.

Calculating the fiber thicknesses from these SEM images for the coated vs. uncoated carbon fabric, the PPy thicknesses for C1-PPy30 and C1-PPy90 range mostly between 0.3 and 1 μm, and 0.8–1.2 μm, respectively. The PPy thickness has a distribution with a maximum value near the outer surface of the carbon fabric and a gradual decrease within its depth. For a more precise picture, energy dispersive X-ray spectroscopy (EDS) was used to approximate the contents of Cl^- counter ions as the distance from the outer surface of carbon fabric is increased in a vertical line (Fig. 2a). Following the trace of Cl^- ions as an indication of PPy coating formation and content, it is observed that PPy was mostly formed up to the first 200 μm depth. After this depth, the coating amount significantly decreased and continued up to around 400 μm.

To quantify the mass of coated PPy in the carbon fabric, TGA was performed between 35 and 750 °C and the result is shown in Fig. 2b. The onset decomposition temperature is around 150 °C, after which the PPy gradually decomposes and shows a significant loss at around 600 °C, in line with a previous report on the decomposition temperature of PPy [52]. It could be inferred that PPy coatings contain a distribution of PPy

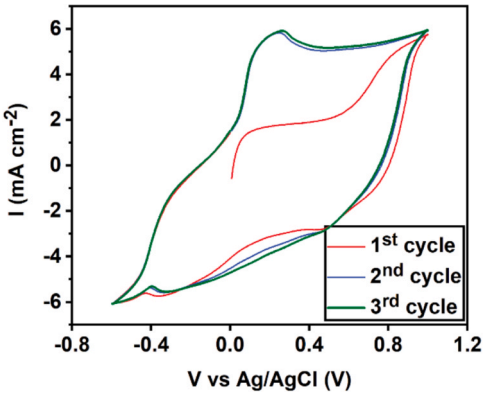

Fig. 6. CV curves of the initial three cycles for C2-PPy90 in H_2SO_4 (1 mol L^{-1}) between − 0.6–1 V.

Table 3
The extracted oxidation and reduction potential of C1-PPy90 obtained from CV measurement in the first three cycles.

Redox potentials	1st cycle	2nd cycle	3rd cycle
E_{pa}	-	0.53	0.52
E_{pc}	0.75, − 0.25	0.16	0.19
ΔE	-	0.37	0.33

oligomers with lower and higher molecular weights; yet the significant chains tend to be at the higher end of the molecular weight distribution of PPy as evidenced by the decomposition temperature as high as 600 °C. This shows the potential of PPy for application in high-temperature electrochemical energy storage devices [53], providing the chains could be all grown in high molecular weights; otherwise, the small portion of PPy decomposition under 200 °C could compromise the safety of an entire device.

3.2. Electrode aging

To investigate how the thickness and morphology of the oCVD-grown PPy impact their long-term performance, the above two electrodes were degraded according to an accelerated electrochemical aging protocol. For a wider voltage stability, $LiClO_4$/PC (0.25 mol L^{-1}) was used as the electrolyte and the electrodes were cycled 1000 times between − 1–1 V. A typical CV scan from these electrodes are presented in Fig. S1. Their capacitance loss per surface area was monitored and shown in Fig. 3. As presented, C1-PPy30 shows a decrease in the first fifty cycles, after which the capacitance loss would be very slow. Interestingly, C1-PPy90 shows about a 400% increase in its initial capacitance at the beginning stage of cycling, followed by a rather sharp decrease of around 200%. It could be hypothesized that upon initial oxidation of the thicker C1-PPy90 electrode, only the outer surface of the electrode is oxidized; though in subsequent cycles, ions "open" new channels into inner PPy depth, resulting in enhanced specific capacitance. Such a behavior has been observed before and attributed to material activation and increased wettability during cycling [54–57]. The electrode shows its maximum capacitance at around 50 cycles, possibly after full activation of the entire PPy coating.

Fig. 3b shows the slope of this capacitance change for both electrodes. The C1-PPy30 electrode shows a steady curve with a slope of almost zero after 300 cycles; while for the C1-PPy90 electrode, it is only after 900 cycles that the slope approaches zero. That said, even if we assume that the capacitance loss continues at the same rate afterward, C1-PPy30 shows a significantly higher degree of stability if the variation between maximum and minimum capacitance is compared after 1000 cycles. This suggests that a lower thickness of PPy on carbon fabric is more stable over time.

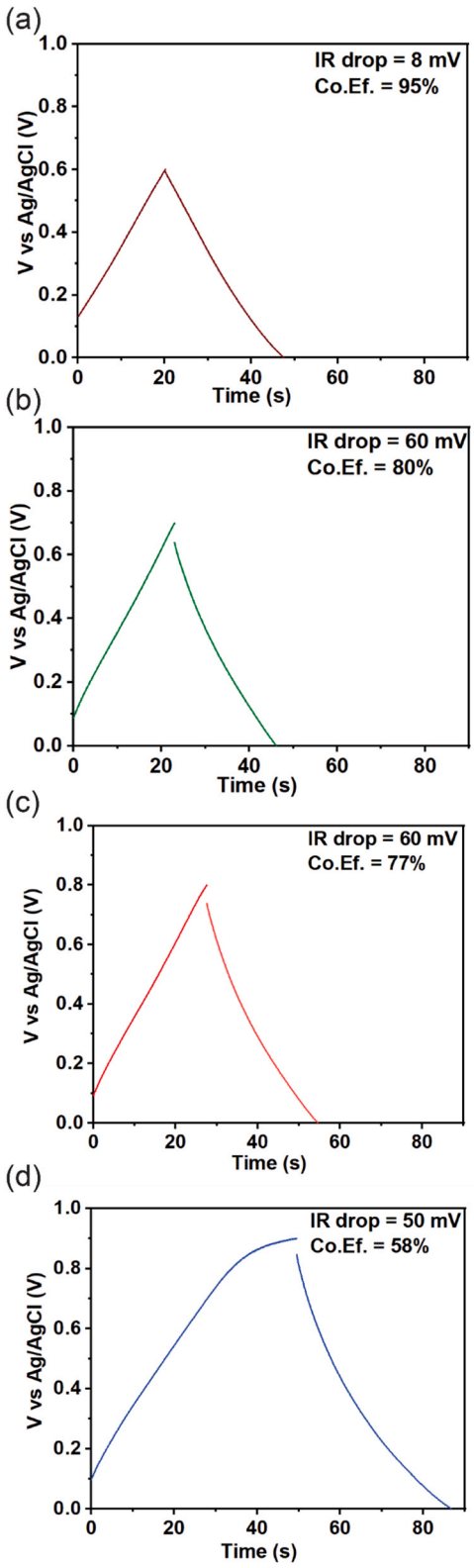

Fig. 7. GCD curve of the 5th cycle for C1-PPy90 electrode with different cut-off voltages of 0.6, 0.7, 0.8, 0.9 V.

SEM micrographs of the electrodes at the end of 100 and 1000 cycles also corroborate the above observation. PPy delamination from the carbon fabric surface should be accounted for as the main reason for the capacitance loss, as seen in Fig. 4. This usually initiates with local cracks

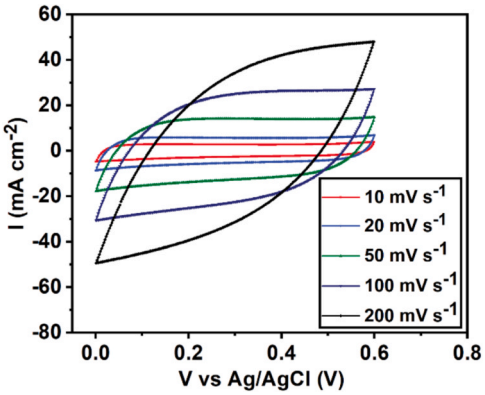

Fig. 8. CV measurement of C2-PPy90 electrode at different scan rates of 10, 20, 50, 100, and 200 mVs^{-1} in H_2SO_4 (1 mol L^{-1}) using three-electrode system.

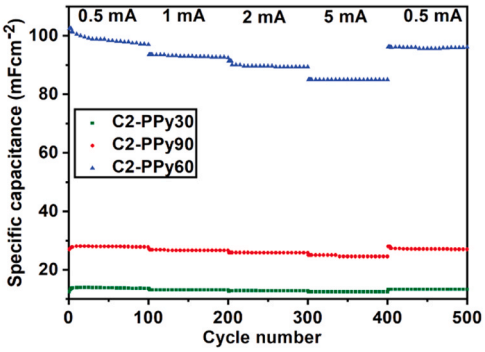

Fig. 9. Areal capacitance evolution of C2-PPy30, C2-PPy60, and C2-PPy90 electrode from GCD measurements with current densities of 0.5, 1, 2, and 5 mA cm^{-2}.

at the surface of PPy. Comparing the graphs of Fig. 4b vs. 4a for the C1-PPy30 electrode with those of the non-degraded ones (Fig. 1), we learn that C1-PPy30 shows very good stability up to 100 cycles. The initiation of a few local cracks is observable, which become obvious when cycled 1000 times (Fig. 4b). Fig. 4c on the other hand shows clear cracking of the PPy shell for 100 times of cycling. These cracks further support the occurrence of the activation of inner PPy bulk in the early stage of cycling, simply because the electrolyte could transport through the depth of PPy more easily. These cracks then connect over time and result in coating failure of the PPy shell, significantly distorting its initial morphology (Fig. 4d). The alteration of morphology and how it facilitates the degradation process of PPy during electrochemical activity has been reported before [58].

In addition to the physical perspective, energy-dispersive X-ray spectroscopy (EDS) could be used to gain insight into chemical evolution of electrode surface in electrochemical energy storage electrodes upon their cycling [59–61]. In this regard, SEM–EDS was performed on unaged electrodes as well as the ones cycled 100 and 1000 times (Fig. 5). As could be observed for C1-PPy30, a small nitrogen peak is detectable, which would disappear for the electrodes cycled 100 and 1000 times (Fig. 5a). Though this is attributed to low sensitivity of EDS in detecting nitrogen in general along with low -"N"- content in a pyrrole unit as well [62]. The general trend in Fig. 5a is the reduction of -"Sb"- and -"Cl"- intensity and appearance and increase of -"O"- intensity, suggesting oxidation of the polymer. The same trend is observable for C1-PPy90 as well. However, using oxygen content as an indicator of PPy over-oxidation, C1-PPy30 shows 11 at% of the entire elements at the end of 1000 times cycling, while for C1-PPy90, this number is as high as 35 at% (Fig. 5b). This further corroborates the above results and suggests that the thicker PPy was not only susceptible to physical deterioration due to delamination, but also chemical degradation because of more severe overoxidation. The effect of thickness on overoxidation needs further investigation.

3.3. Energy storage performance

We designed experiments to assess the electrochemical energy storage behavior of PPy-carbon fabric. The results from the degradation experiments partly suggest that a wide voltage range up to 1 V resulted in significant capacitance fade in long-term cycling. In this regard, a lower voltage range is to be found for the optimized performance of these electrode. Additionally, in lower voltage thresholds, aqueous electrolytes are preferable due to their higher ionic conductivity among all electrolyte types [63]. Following this, the carbon fabric was first thermally oxidized to improve its wettability in aqueous environment (details in Experimental), and then coated with PPy for 30, 60, and 90 min, resulting in C2-PPy30, C2-PPy60, and C2-PPy90, respectively. Similarly, TGA curves were used to calculate the PPy mass content per mass of the carbon fabric-PPy electrodes (Fig. S2). Interestingly, it is observed that compared to the previous set of experiments, the mass percentage for PPy was increased to 4, 5, and 6 wt% of the electrodes for C2-PPy30, C2-PPy60, and C2-PPy90 electrodes, respectively (measured

Table 4
Comparison between supercapacitive performance of carbon fabric-PPy electrode developed in this work with a few similar reports.

Electrode	Electrolyte	Gravimetric capacitance (F g^{-1})	Areal capacitance (mF cm^{-2})	Voltage range	Current density/ scan rate	Capacitance retention	Measurement type	scale	Reference
PPy	H_2SO_4 (0.1 mol L^{-1})	-	50–120	0–1 V	10–50 mV s^{-1}	-	3-electrode	1 cm^2	[66]
PPy/GO	H_2SO_4 (1 mol L^{-1})	332	-	-0.2–0.8 V	5 mV s^{-1}	-	2-electrode	1 cm^2, 180 μg PPy	[65]
PPy/ carbon nano-onion	ACN/ $LiClO_4$ (0.1 mol L^{-1})	1320	-	-0.1–0.2 V vs. Ag/AgCl	20 mV s^{-1}	80% @ 500 cycles	3-electrode	7.1 μg cm^{-1}	[52]
PPy/CoNi LDH core-shell	KOH (1 mol L^{-1})	1137	-	0–0.5 V vs. SCE	1 A g^{-1}	90% @ 2000 cycles	3-electrode	1.4 mg	[67]
PPy/carbon cloth	H_2SO_4 (1 mol L^{-1})	469	210	0–0.8 V vs. Ag/AgCl	1 mA cm^{-2}	85% @ 5000 cycles	3-electrode	1 cm^2	[68]
PPy/activated carbon	Na_2SO_4 (1 mol L^{-1})	131	-	0–1 V	0.5 A g^{-1}	-	2-electrode	2 mg	[69]
PPy/graphene/ carbon nanotube	KCl (1 mol L^{-1})	-	196	0–0.8 V	0.5 mA cm-2	98% @ 5000 cycles	2-electrode	Not clear	[70]
PPy/ microporous carbon fiber	H_2SO_4 (1 mol L^{-1})	209	102	0–0.6 V vs. Ag/AgCl	0.5 mA cm^{-2}	(93-)100% after 500 cycles	3-electrode	1 cm^2	Our work

by TGA mass loss around 600 °C). This shows a 50% increase in the deposition rate of PPy and could primarily be attributed to a favorable interaction of oxidant/monomer with thermally-oxidized carbon fabric. Yet, the substrate thermal oxidation did not have any effect on morphology growth of PPy, which suggests that the polymer morphology is in principle dictated by oCVD process and film thickness (Fig. S3).

Cyclic voltammetry was performed on C2-PPy90 electrode in H_2SO_4 (1 mol L^{-1}) between − 0.6–1 V vs. Ag/AgCl for three cycles and the result is presented in Fig. 6. As observed, during the first cycle, which started at 0 V, the current quickly increased to 2 mA and continued increasing up to around 0.6 V, after which it showed deviation from the ideal rectangular like CV behavior up to 1 V. Within the same cycle and upon reduction, the curve shows two broad peaks at 0.75 V and − 0.25 V. However, in the 2nd cycle, the CV curve shows an oxidation potential maximum (E_{pa}) at 0.53 V and a reduction peak maximum (E_{pc}) at 0.16 V. This suggests a reversible redox reaction with a peak-to-peak separation of only 0.37 V, which becomes even smaller in the 3rd cycle (Table 3). The lower end voltage threshold of this electrode that shows capacitive-like behavior is − 0.4 V; though on the higher end, it seems like the voltage cut-off could be stretched up to 0.9 V from the 2nd cycle. This is a 0.3 V difference compared with the 1st cycle.

In order to determine the safe working voltage range for these electrodes more accurately, galvanostatic charge-discharge (GCD) experiment was performed on a newly prepared C2-PPy90 electrode with cut-off voltage of 0.6, 0.7, 0.8, and 0.9 V for five cycles. The data from the 5th cycle for each cut-off voltage is presented in Fig. 7. The data for each experiment is compared against IR drop and Coulombic efficiency. As could be noticed, except the cut-off voltage of 0.6 V, the others show a very low (< 80%) Coulombic efficiency with about one order of magnitude higher IR drop. This strongly suggests that, irrespective of CV results, the optimal voltage range for electrochemical charge and discharge of C-PPy electrode is a maximum of 0.6 V. Besides, for the cut off-voltage of 0.9 V, it is observed that the charging curve deviates from capacitive-like behavior at above 0.8 V, resembling battery-like behavior [64].

Subsequently, CV data was collected for a C2-PPy90 electrode (1 cm^2) between 0 and 0.6 V for different scan rates from 10 mV s^{-1} to 500 mV s^{-1} (Fig. 8). As could be observed, at lower scan rates up to 50 mV s^{-1}, the CV curve has a rectangular-like shape which become more cone-like at higher scan rates up to 500 mV s^{-1}. This is a typical and accepted supercapacitive behavior, corroborating the previous conclusion from GCD results on voltage threshold [65].

Building upon the above foundation, the capacitance of C2-PPy30, C2-PPy60, and C2-PPy90 were evaluated using GCD for current densities of 0.5 mA cm^{-2} to 5 mA cm^{-2} and the results are presented in Fig. 9. As could be seen, the C2-PPy30 electrode shows an initial specific capacitance of 12 mF cm^{-2}, which significantly increases to about 102 mF cm^{-2} for C2-PPy60. Interestingly, it decreases again for the C2-PPy90 electrode in spite of its higher PPy content/thickness. This shows that with increasing the thickness of PPy, the capacitance would initially enhance as a result of higher gravimetric density of PPy. Though if the thickness surpasses a critical point, the capacitance will decrease again, possibly as a result of longer travel distance for the ions. In terms of stability, both C2-PPy30 and C-PPy90 showed 100% capacitance retention after 500 cycles, though for C2-PPy60, it shows a 7% reduction of specific capacitance when comparing the 500th to the first cycle. The reason behind such a behavior is not entirely clear; since if the higher thickness of C2-PPy60 is prompting its higher degradation rate, this should be even more intense in the case of C2-PPy90. One interpretation could be that the PPy thickness has an indirect consequence on electrode degradation during cycling. In other words, if a higher thickness of PPy hinders the electrochemical reaction, it results in a lower deterioration as well simply because of lower electrochemical activation.

Finally, comparing the results obtained in this report with those of literature (Table 4), it can be concluded that the capacitance obtained in this work is comparable with the ones which used microporous electrode structures in their work. The improved performance in some reports is most likely a result of the smaller length scale and/or nanostructure, which the specific surface area of electrode and electrolyte-electrode interface. This strategy is also previously reported in oCVD application for supercapacitors [43]. Further research in this trajectory is out of scope for the current work, though it is suggested as a logical next step.

4. Conclusion

In summary, this work provides the first report on oCVD grown PPy for electrochemical energy storage applications. oCVD was used for the one-step synthesis of PPy on a commercially available carbon fabric and the composite could be used as a supercapacitive electrode. The deposited PPy adheres to the 3D microstructure of carbon fiber and contributes to charge transport at the interface while maintaining a high surface area microporous geometry. The performance of the developed electrode is comparable with other reports, which use a microporous substrate. The effect of the PPy coating thickness on areal specific capacitance revealed that with increasing PPy thickness, the capacitance would initially increase due to a higher PPy content. However, if the PPy thickness exceeds a critical point, the capacitance starts to decrease due to the long diffusion path of ions. Electrode stability however, does not appear to have a direct association with the PPy coating thickness, but to redox activity as a result of thickness. In the above results, when a higher thickness was associated with higher capacitance (we consider it as higher redox activity), the coating also degraded more. However, a larger increase in thickness resulted in a lower capacitance and hence redox activity, which showed itself with less degradation rate. This aspect needs more investigation.

For further research, the directions that could be suggested are using nanoporous substrates and exploit the advantage of oCVD for deposition of polymer coatings at the nanoscale. Additionally, the advances in the field of conjugated polymers for electrochemical energy storage applications should focus on improving the stability of PPy. Two immediate directions could be deposition of a thin protective layer on top of PPy, and/or co-deposition of PPy with conjugated polymer containing an alkyl side chain, thus providing a higher level of flexibility within the polymer coating and during constant shrinkage/expansion.

CRediT authorship contribution statement

Afshin Dianatdar: Conceptualization, Methodology, Validation, Formal analysis, Investigation, Data curation, Writing – original draft, Visualization. **Adrivit Mukherjee:** Data curation, Writing – review & editing. **Ranjita K. Bose:** Supervision, Writing – review & editing, Resources, Project administration.

Declaration of Competing Interest

The authors declare that they have no known competing financial interests or personal relationships that could have appeared to influence the work reported in this paper.

Data Availability

Data will be made available on request.

Acknowledgement

The authors would like to thank Dr. Matteo Miola for the constructive discussions and support for the electrochemical experiments of current work.

Appendix A. Supporting information

Supplementary data associated with this article can be found in the online version at doi:10.1016/j.synthmet.2023.117444.

References

[1] N. Khan, S. Dilshad, R. Khalid, A.R. Kalair, N. Abas, Review of energy storage and transportation of energy, Energy Storage 1 (2019) 1–49.
[2] A.Z. AL Shaqsi, K. Sopian, A. Al-Hinai, Review of energy storage services, applications, limitations, and benefits, Energy Rep. 6 (2020) 288–306.
[3] S. Ratha, A.Kumar Samantara, 2018. Supercapacitor: instrumentation, measurement and performance evaluation techniques, 2018.
[4] M. Winter, R.J. Brodd, What are batteries, fuel cells, and supercapacitors? Chem. Rev. 104 (2004) 4245–4269.
[5] K.K. Kar, Springer series in materials science 300 handbook of nanocomposite supercapacitor materials I, 2020.
[6] J. Zhao, A.F. Burke, Review on supercapacitors: technologies and performance evaluation, J. Energy Chem. 59 (2021) 276–291.
[7] B.K. Kim, S. Sy, A. Yu, J. Zhang, Electrochemical supercapacitors for energy storage and conversion, Handb. Clean. Energy Syst. (2015) 1–25.
[8] Y. Jiang, J. Liu, Definitions of pseudocapacitive materials: a brief review, Energy Environ. Mater. 2 (2019) 30–37.
[9] P. Sharma, T.S. Bhatti, A review on electrochemical double-layer capacitors, Energy Convers. Manag 51 (2010) 2901–2912.
[10] I. Shown, A. Ganguly, L.C. Chen, K.H. Chen, Conducting polymer-based flexible supercapacitor, Energy Sci. Eng. 3 (1) (2015) 25.
[11] M.A.A. Mohd Abdah, N.H.N. Azman, S. Kulandaivalu, Y. Sulaiman, Review of the use of transition-metal-oxide and conducting polymer-based fibres for high-performance supercapacitors, Mater. Des. 186 (2020), 108199.
[12] J.F. Mike, J.L. Lutkenhaus, Recent advances in conjugated polymer energy storage, J. Polym. Sci. B Polym. Phys. 51 (2013) 468–480.
[13] B. Szubzda, A. Szmaja, M. Ozimek, S. Mazurkiewicz, Polymer membranes as separators for supercapacitors, Appl. Phys. A Mater. Sci. Process 117 (2014) 1801–1809.
[14] X. Cheng, J. Pan, Y. Zhao, M. Liao, H. Peng, Gel polymer electrolytes for electrochemical energy storage, Adv. Energy Mater. 8 (2018), 1702184.
[15] T. Le, H. Yoon, Conjugated polymer nanostructures for electrochemical capacitor and lithium-ion battery applications, Conjug. Polym. Nanostruct. Energy Convers. Storage Appl. (2021) 357–400.
[16] J. Wang, S. Dong, B. Ding, Y. Wang, X. Hao, H. Dou, Y. Xia, X. Zhang, Pseudocapacitive materials for electrochemical capacitors: From rational synthesis to capacitance optimization, Natl. Sci. Rev. 4 (2017) 71–90.
[17] Y. Huang, H. Li, Z. Wang, M. Zhu, Z. Pei, Q. Xue, Y. Huang, C. Zhi, Nanostructured polypyrrole as a flexible electrode material of supercapacitor, Nano Energy 22 (2016) 422–438.
[18] J. El Nady, A. Shokry, M. Khalil, S. Ebrahim, A.M. Elshaer, M. Anas, One-step electrodeposition of a polypyrrole/NiO nanocomposite as a supercapacitor electrode, Sci. Rep. 12 (2022) 3611.
[19] A. Shokry, M. Karim, M. Khalil, S. Ebrahim, J. El Nady, Supercapacitor based on polymeric binary composite of polythiophene and single-walled carbon nanotubes, Sci. Rep. 12 (2022) 11278.
[20] A. Eftekhari, L. Li, Y. Yang, Polyaniline supercapacitors, J. Power Sources 347 (2017) 86–107.
[21] A. Laforgue, P. Simon, C. Sarrazin, J.-F. Fauvarque, Polythiophene-based supercapacitors, J. Power Sources 80 (1999) 142–148.
[22] A.K. Thakur, M. Majumder, R.B. Choudhary, S.N. Pimpalkar, 2016. Supercapacitor based on electropolymerized polythiophene and multiwalled carbon nanotubes composites, Conference Series: Mater Sci Eng. 149 (2016) 012166.
[23] Electric double-layer capacitors for use in hybrid electric vehicles - Test methods for electrical characteristics, International Standard. ⟨https://webstore.iec.ch/publication/62711⟩.
[24] J. Heinze, B.A. Frontana-Uribe, S. Ludwigs, Electrochemistry of conducting polymers-persistent models and new concepts, Chem. Rev. 110 (2010) 4724–4771.
[25] Q. Wu, T. He, Y. Zhang, J. Zhang, Z. Wang, Y. Liu, L. Zhao, Y. Wu, F. Ran, Cyclic stability of supercapacitors: materials, energy storage mechanism, test methods, and device, J. Mater. Chem. A Mater. 9 (2021) 24094–24147.
[26] S. Biswas, L.T. Drzal, Multilayered nanoarchitecture of graphene nanosheets and polypyrrole nanowires for high performance supercapacitor electrodes, Chem. Mater. 22 (2010) 5667–5671.
[27] J. Zhang, X.S. Zhao, Conducting polymers directly coated on reduced graphene oxide sheets as high-performance supercapacitor electrodes, J. Phys. Chem. C. 116 (2012) 5420–5426.
[28] Y. Liu, H. Wang, J. Zhou, L. Bian, E. Zhu, J. Hai, J. Tang, W. Tang, Graphene/polypyrrole intercalating nanocomposites as supercapacitors electrode, Electro Acta 112 (2013) 44–52.
[29] C. Xia, W. Chen, X. Wang, M.N. Hedhili, N. Wei, H.N. Alshareef, Highly stable supercapacitors with conducting polymer core-shell electrodes for energy storage applications, Adv. Energy Mater. 5 (2015), 1401805.
[30] T. Liu, L. Finn, M. Yu, H. Wang, T. Zhai, X. Lu, Y. Tong, Y. Li, Polyaniline and polypyrrole pseudocapacitor electrodes with excellent cycling stability, Nano Lett. 14 (2014) 2522–2527.
[31] M.A. del Valle, M.A. Gacitúa, F. Hernández, M. Luengo, L.A. Hernández, Nanostructured conducting polymers and their applications in energy storage devices, Polymers 15 (2023) 1450.
[32] D.S. Patil, J.S. Shaikh, D.S. Dalavi, S.S. Kalagi, P.S. Patil, Chemical synthesis of highly stable PVA/PANI films for supercapacitor application, Mater. Chem. Phys. 128 (2011) 449–455.
[33] J.S. Shayeh, P. Norouzi, M.R. Ganjali, Effect of thickness on the capacitive behavior and stability of ultrathin polyaniline for high speed super capacitors, Russ. J. Electrochem. 52 (2016) 933–937.
[34] G.Z. Chen, Understanding supercapacitors based on nano-hybrid materials with interfacial conjugation, Prog. Nat. Sci.: Mater. Int. 23 (2013) 245–255.
[35] K.U. Lee, J.Y. Byun, H.J. Shin, S.H. Kim, A high-performance supercapacitor based on polyaniline-nanoporous gold, J. Alloy. Compd. 779 (2019) 74–80.
[36] S.L. Pittelli, D.E. Shen, A.M. Österholm, J.R. Reynolds, Chemical oxidation of polymer electrodes for redox active devices: stabilization through interfacial interactions, ACS Appl. Mater. Interfaces 10 (2018) 970–978.
[37] X. Wang, Y. Yang, C. Lai, R. Li, H. Xu, D.H.S. Tan, K. Zhang, W. Yu, O. Fjeldberg, M. Lin, W. Tang, Y.S. Meng, K.P. Loh, Dense-stacking porous conjugated polymer as reactive-type host for high-performance lithium sulfur batteries, Angew. Chem. - Int. Ed. 60 (2021) 11359–11369.
[38] Y.Y. Smolin, K.L. Van Aken, M. Boota, M. Soroush, Y. Gogotsi, K.K.S. Lau, Engineering ultrathin polyaniline in micro/mesoporous carbon supercapacitor electrodes using oxidative chemical vapor deposition, Adv. Mater. Interfaces 4 (2017), 1601201.
[39] K.K. Gleason, Overview of Chemically Vapor Deposited (CVD) polymers, CVD Polym.: Fabr. Org. Surf. Devices 1 (2015) 1–11.
[40] D.E. Weidner, L.W. Schwartz, R.R. Eley, Role of surface tension gradients in correcting coating defects in corners, J. Colloid Interface Sci. 179 (1996) 66–75.
[41] F. Zhang, G. Baralia, A. Boborodea, C. Bailly, B. Nysten, A.M. Jonas, Partial dewetting of polyethylene thin films on rough silicon dioxide surfaces, Langmuir 21 (2005) 7427–7432.
[42] M. Ghaffari, S. Kosolwattana, Y. Zhou, N. Lachman, M. Lin, D. Bhattacharya, K. K. Gleason, B.L. Wardle, Q.M. Zhang, Hybrid supercapacitor materials from poly (3,4-ethylenedioxythiophene) conformally coated aligned carbon nanotubes, Electro Acta 112 (2013) 522–528.
[43] Y. Zhou, N. Lachman, M. Ghaffari, H. Xu, D. Bhattacharya, P. Fattahi, M. R. Abidian, S. Wu, K.K. Gleason, B.L. Wardle, Q.M. Zhang, A high performance hybrid asymmetric supercapacitor via nano-scale morphology control of graphene, conducting polymer, and carbon nanotube electrodes, J. Mater. Chem. A Mater. 2 (2014) 9964–9969.
[44] Y. Zhou, H. Xu, N. Lachman, M. Ghaffari, S. Wu, Y. Liu, A. Ugur, K.K. Gleason, B. L. Wardle, Q.M. Zhang, Advanced asymmetric supercapacitor based on conducting polymer and aligned carbon nanotubes with controlled nanomorphology, Nano Energy 9 (2014) 176–185.
[45] A. Liu, P. Kovacik, N. Peard, W. Tian, H. Goktas, J. Lau, B. Dunn, K.K. Gleason, Monolithic Flexible Supercapacitors Integrated into Single Sheets of Paper and Membrane via Vapor Printing, Adv. Mater. 29 (2017), 1606091.
[46] Y.Y. Smolin, M. Soroush, K.K.S. Lau, Influence of oCVD polyaniline film chemistry in carbon-based supercapacitors, Ind. Eng. Chem. Res 56 (2017) 6221–6228.
[47] Y. Zhou, X. Wang, L. Acauan, E. Kalfon-Cohen, X. Ni, Y. Stein, K.K. Gleason, B. L. Wardle, Ultrahigh-areal-capacitance flexible supercapacitor electrodes enabled by conformal P3MT on horizontally aligned carbon-nanotube arrays, Adv. Mater. 31 (2019), 1901916.
[48] A. Dianatdar, M. Miola, O. De Luca, P. Rudolf, F. Picchioni, R. Bose, All-Dry, one-step synthesis, doping and film formation of conductive polypyrrole, J. Mater. Chem. C. 10 (2022) 557–570.
[49] N.C.T. Martins, T. Moura e Silva, M.F. Montemor, J.C.S. Fernandes, M.G. S. Ferreira, Electrodeposition and characterization of polypyrrole films on aluminium alloy 6061-T6, Electro Acta 53 (2008) 4754–4763.
[50] T. Patois, B. Lakard, S. Monney, X. Roizard, P. Fievet, Characterization of the surface properties of polypyrrole films: Influence of electrodeposition parameters, Synth. Met. 161 (2011) 2498–2505.
[51] Z. Zhang, Y. Song, J. Xu, N. Li, Z. Tang, L. Xu, J. Du, Facile synthesis of p-toluene sulfonic acid doped polypyrrole films for bifunctional electrochromic supercapacitor application, Mater. Express 11 (2021) 344–352.
[52] O. Mykhailiv, M. Imierska, M. Petelczyc, L. Echegoyen, M.E. Plonska-Brzezinska, Chemical versus electrochemical synthesis of carbon nano-onion/polypyrrole composites for supercapacitor electrodes, Chem. - A Eur. J. 21 (2015) 5783–5793.
[53] X. Lin, M. Salari, L.M.R. Arava, P.M. Ajayan, M.W. Grinstaff, High temperature electrical energy storage: advances, challenges, and frontiers, Chem. Soc. Rev. 45 (2016) 5848–5887.
[54] X. Li, A. Rafie, Y.Y. Smolin, S. Simotwo, V. Kalra, K.K.S. Lau, Engineering conformal nanoporous polyaniline via oxidative chemical vapor deposition and its potential application in supercapacitors, Chem. Eng. Sci. 194 (2019) 156–164.
[55] J. Zhou, J. Lian, L. Hou, J. Zhang, H. Gou, M. Xia, Y. Zhao, T.A. Strobel, L. Tao, F. Gao, Ultrahigh volumetric capacitance and cyclic stability of fluorine and nitrogen co-doped carbon microspheres, Nat. Commun. 6 (2015) 8503.
[56] C. Zequine, C.K. Ranaweera, Z. Wang, S. Singh, P. Tripathi, O.N. Srivastava, B. K. Gupta, K. Ramasamy, P.K. Kahol, P.R. Dvornic, R.K. Gupta, High per formance and flexible supercapacitors based on carbonized bamboo fibers for wide temperature applications, Sci. Rep. 6 (1) (2016) 10.
[57] A. Gigot, M. Fontana, C.F. Pirri, P. Rivolo, Graphene/ruthenium active species aerogel as electrode for supercapacitor applications, Materials 11 (1) (2017) 12.
[58] B.M. Hryniewicz, R.V. Lima, L.F. Marchesi, M. Vidotti, Impedimetric studies about the degradation of polypyrrole nanotubes during galvanostatic charge and discharge cycles, J. Electroanal. Chem. 855 (2019), 113636.

[59] N. Wu, H. Wu, H. Liu, Y. Zhang, Solvothermal coating LiNi0.8Co0.15Al0.05O2 microspheres with nanoscale Li2TiO3 shell for long lifespan Li-ion battery cathode materials, J. Alloy. Compd. 665 (2016) 48–56.
[60] J. Park, G.H. An, Interface-engineered electrode and electrolyte for the improved energy-storing performance and stable mechanical flexibility of fibrous supercapacitors, Appl. Surf. Sci. 549 (2021), 149326.
[61] G. Yoo, B.R. Koo, G.H. An, Nano-sized split V2O5 with H2O-intercalated interfaces as a stable cathode for zinc ion batteries without an aging process, Chem. Eng. J. 434 (2022), 134738.
[62] W.J. Wolfgong, Chapter 14 - Chemical analysis techniques for failure analysis: Part 1, common instrumental methods, in: Handbook of Materials Failure Analysis with Case Studies from the Aerospace and Automotive Industries, 2016: pp. 279–307.
[63] B. Pal, S. Yang, S. Ramesh, V. Thangadurai, R. Jose, Electrolyte selection for supercapacitive devices: a critical review, Nanoscale Adv. 1 (2019) 3807–3835.
[64] T.S. Mathis, N. Kurra, X. Wang, D. Pinto, P. Simon, Y. Gogotsi, Energy storage data reporting in perspective—guidelines for interpreting the performance of electrochemical energy storage systems, Adv. Energy Mater. 9 (2019) 1–13.
[65] I.M. De La Fuente Salas, Y.N. Sudhakar, M. Selvakumar, High performance of symmetrical supercapacitor based on multilayer films of graphene oxide/polypyrrole electrodes, Appl. Surf. Sci. 296 (2014) 195–203.
[66] M.S. Kumar, D.K. Bhat, LiClO4-doped plasticized chitosan as biodegradable polymer gel electrolyte for supercapacitors, J. Appl. Polym. Sci. 114 (2009) 2445–2454.
[67] M. Shao, Z. Li, R. Zhang, F. Ning, M. Wei, D.G. Evans, X. Duan, Hierarchical conducting Polymer@Clay core-shell arrays for flexible all-solid-state supercapacitor devices, Small 11 (2015) 3530–3538.
[68] Z. Yang, Z. Chen, Thermally doped polypyrrole nanotubes with sulfuric acid for flexible all-solid-state supercapacitors, Nanotechnology 30 (2019), 245402.
[69] A. Bello, F. Barzegar, M.J. Madito, D.Y. Momodu, A.A. Khaleed, T.M. Masikhwa, J. K. Dangbegnon, N. Manyala, Electrochemical performance of polypyrrole derived porous activated carbon-based symmetric supercapacitors in various electrolytes, RSC Adv. 6 (2016) 68141–68149.
[70] H. Zhou, H.J. Zhai, X. Zhi, Enhanced electrochemical performances of polypyrrole/carboxyl graphene/carbon nanotubes ternary composite for supercapacitors, Electro Acta 290 (2018) 1–11.